Theor Chem Acc (2004) 111:363–372
DOI 10.1007/s00214-003-0528-1

Theoretical
Chemistry Accounts

*Regular article*

# A theoretical study of the lowest electronic states of azobenzene: the role of torsion coordinate in the cis–trans photoisomerization

**Laura Gagliardi**[1], **Giorgio Orlandi**[2], **Fernando Bernardi**[2], **Alessandro Cembran**[2], **Marco Garavelli**[2]

[1] Dipartimento di Chimica Fisica F. Accascina, Università di Palermo, Viale delle Scienze, Parco d'Orleans II, Pad. 17, 90128, Palermo, Italy
[2] Dipartimento di Chimica G. Ciamician, Università di Bologna, Via F. Selmi 2, 40126 Bologna, Italy

Received: 13 February 2003 / Accepted: 24 May 2003 / Published online: 8 December 2003


**Abstract.** In the present paper we report the results of a multiconfigurational computational study on potential-energy curves of azobenzene along the NN twisting to clarify the role of this coordinate in the decay of the $S_2(\pi\pi^*)$ and $S_1(n\pi^*)$ states. We have found that there is a singlet state, $S_3$ at the trans geometry, on the basis of the doubly excited configuration $n^2\pi^{*2}$, that has a deep minimum at about 90° of twisting, where it is the lowest excited singlet state. The existence of this state provides an explanation for the short lifetime of $S_2(\pi\pi^*)$ and for the wavelength-dependence of azobenzene photochemistry. We have characterized the $S_1(n\pi^*)$ state by calculating its vibrational frequencies, which are found to correspond to the recently observed transient Raman spectrum. We have also computed the potential-energy curve for the triplet $T_1(n\pi^*)$ at the density functional theory B3LYP level, which indicates that in this state the isomerization occurs along the twisting coordinate.

**Keywords:** Azobenzene – Excited electronic states – Photoisomerization – Multiconfigurational wave function methods

## Introduction

Azobenzene (Ab) and many of its derivatives undergo cis–trans isomerization both photochemically and thermally [1, 2]. Cis (Z) and trans (E) isomers exhibit well-separated absorption bands in the UV–vis region [1, 2] and thus each isomer can be easily photoconverted into the other. Since the two isomers have, in general, different physical properties, such as dielectric constant and refractive index, Ab and its derivatives are good candidates for many applications as light-triggered switches [3]. Molecular systems based on Ab can be used as constituents of erasable holographic data, image storage devices and materials with photomodulable properties [4, 5, 6]. Furthermore, it has recently been proposed that the Ab photoisomerization could be a basis for a light-powered molecular machine [7]. For these reasons Ab has been the subject of an intense study and a detailed understanding of its photochemistry may result in many useful applications in material science.

The UV–vis absorption spectrum of *E*-Ab in hexane solution shows a weak band at 432 nm ($\epsilon_{max} = 400$) and an intense band with a maximum at 318 nm ($\epsilon_{max} = 22{,}300$) [3, 8, 9, 10, 11, 12]. The former is structureless even in low-temperature mixed crystals [13, 14] and is attributed to the lowest singlet state, $S_1$, of $n\pi^*$ nature and of $B_g$ type in the $C_{2h}$ symmetry group. The latter shows a rich vibronic structure in the dibenzyl single-crystal spectrum at 20 K [14], exhibiting identifiable vibrational progressions built upon an origin at 362 nm (27,662 $cm^{-1}$) and is attributed to the $S_2$ state, of $\pi\pi^*$ nature and of $B_u$ symmetry type. Thus, the $S_2 \leftarrow S_0$ transition is allowed, while the $S_1 \leftarrow S_0$ transition is symmetry-forbidden and acquires weak intensity via out-of-plane motions, primarily the twisting around CN bonds. In the *Z*-Ab isomer, one finds similarly two bands in the UV–vis absorption spectrum, at 440 and 260 nm [3], with similar intensity ratio as in *E*-Ab.

The Z–E photoisomerization quantum yield depends on the excitation wavelength [3]. In an inert solvent such as *n*-hexane, the quantum yields of the *E*-Ab → *Z*-Ab photoconversion are 0.25 and 0.12, exciting the $S_1$ and $S_2$ states [15], respectively. The quantum yields of the

Contribution to the Jacopo Tomasi Honorary Issue

*Correspondence to:* G. Orlandi
e-mail: gorlandi@ciam.unibo.it

inverse process *Z*-Ab → *E*-Ab are 0.53 and 0.40, exciting the $S_1$ and $S_2$ states, respectively [15, 16].

Whereas the Z–E isomerization in stilbene, and, in general, in diarylethylenes, takes place along the torsion around the ethylenic double bond, the same process in Ab can proceed along two paths, the torsion around the N=N double bond and the in-plane inversion. In the latter case, the transition state corresponds to a linear geometry whereby one nitrogen atom is *sp* hybridized. The analysis of the photoreactivity of Ab is complicated also by the presence of $n\pi^*$ ($S_1$) and $\pi\pi^*$ ($S_2$) states in the low-energy region of the spectrum. The lifetime of these states is very short (in hexane 0.11 and 0.5 ps for $S_2$ and $S_1$, respectively [17]) and their fluorescence emission is very weak (in hexane the fluorescence quantum yields have been estimated to be $2.5\times10^{-5}$ and $7.5\times10^{-7}$ for $S_2$ and $S_1$, respectively [17]). A specific feature of the Ab photoisomerization is the excitation-wavelength dependence of its quantum yield: the quantum yield is lower when UV light is used for excitation [3]. However, Ab derivatives in which the torsional motion is prohibited show a photoisomerization quantum yield that is the same for both states and which is very similar to the yield of the photoisomerization of Ab excited in $S_1$ [2]. This observation implies that the decay from $S_2$ does not proceed exclusively through $S_1$ and suggests that the photoreaction occurs along different paths in the two states, namely the NN torsion in $S_2$ and along the inversion in the $S_1$ state. This view was confirmed by an early ab initio minimal basis set calculation, performed at selected geometries for the ground state and a few excited states ($S_0$, $S_1$, $S_2$, $T_1$, $T_2$) [18], which provided the first potential-energy diagram to discuss the photophysical observations on Ab. Recently, Cattaneo and Persico [19] have reconsidered the photochemistry of Ab following the $^1n\pi^*$ and $^1\pi\pi^*$ excitation and the thermal isomerization of Ab at the complete-active-space self-consistent-field (CASSCF) level of theory and by multireference perturbation theory at the configuration interaction by perturbation with multiconfigurational zeroth-order wave functions selected by an iterative method (CIPSI) level considering both pathways. They confirmed the view that isomerization occurs along the inversion and the torsion path upon excitation of $S_1$ and $S_2$, respectively. They also found a totally symmetric excited state, based on a doubly excited configuration, showing a potential-energy minimum along the torsion, at about 90°. This state, which can be reached from $S_2$ by overcoming an energy barrier, suggests that the torsion coordinate may play a significant role in the decay from this state.

Many theoretical studies have been performed by several groups to obtain improved structural, vibrational and energetic information on Ab. Tsuji et al. [20] determined the structure of the ground state of *E*-Ab using second-order Møller–Plesset perturbation theory (MP2) and density functional theory (DFT) methods. CASSCF and multireference configuration interaction with singles and double excitations (MRSDCI) calculations were also performed by Ishikawa et al. [21] to study the $^1n\pi^*$ and $^1\pi\pi^*$ excitations. Very recently, Hättig and Hald [22] tested their newly implemented RI-CC2 triplet excitation energies method on *E*-Ab and determined the energies of the $S_1$ and $T_1$ states.

Several experimental studies have been performed to elucidate the mechanisms of the photophysical and photochemical processes. Femtosecond time-resolved absorption [9, 10, 11, 12] and fluorescence [17] spectra have been measured to clarify the relaxation processes and picosecond time-resolved Raman scattering spectra [23] have been recorded to identify transient intermediate states.

The early photophysical study by Morgante and Struve [24] observed for the first time faint vestiges of $S_1$ and $S_2$ fluorescence spectra. Subsequent studies by Lednev and coworkers [10, 12] by femtosecond UV–vis absorption spectroscopy of *E*-Ab in *n*-hexane solutions revealed a transient absorption at 400 nm with a lifetime ranging from 2.5 ps, by excitation close to the $S_1$ origin, at 503 nm, to 0.6 ps upon excitation well above the $S_1$ origin, at 390 or 420 nm. Excitation in the $S_2$ state, at 300 nm, resulted in a transient absorption around 475 nm with a lifetime shorter than 0.2 ps, associated with the $S_2$ state itself. A time-resolved absorption study was also performed for the Z isomer and, upon excitation in the $S_1$ band, at 435 nm, a photoproduct with a dominant decay of 0.17 ps and a weaker component of 2 ps was found [11].

Very recently Fujino et al. [17] investigated the relaxation mechanism of *E*-Az by femtosecond time-resolved fluorescence following excitation at 280 nm, which corresponds to the blue side of the $S_2 \leftarrow S_0$ absorption. Collecting emissions at several wavelengths, they measured the time-resolved fluorescence spectra and found that the emissions decay according to exponentials described by $\tau_1$ and $\tau_2$, with $\tau_1 = 0.5$ ps and $\tau_2 = 0.11$ ps. The latter lifetime was associated with the $S_2$ decay, while the former was attributed to the $S_1$ decay. In the same paper, these authors estimated that *E*-Ab, excited in $S_2$, decays to $S_1$ with a quantum yield close to unity and, by assuming that *E*-Ab, excited in $S_2$, can decay to $S_1$ only from planar geometries and that it would bypass $S_1$ in the decay from twisted geometries, concluded that *E*-Ab, excited in $S_2$, does not twist around the NN bond and thus cannot isomerize along this path. Thus, Fujino et al. [17] have questioned the generally accepted view that photoisomerization in Ab occurs via inversion in $S_1$ and via rotation in $S_2$, and proposed instead that this photoreaction proceeds via inversion, without participation of the NN twisting, in all electronic states. Clearly, despite the active experimental and theoretical research carried out in recent years, the photoisomerization mechanism in Ab remains unclear. Because of this, we started to reexamine the mechanism of the Ab photoisomerization in the singlet manifold by up-to-date theoretical methods.

Z–E photoisomerization in Ab is also observed by excitation of triplet states [15, 25]. In analogy with the singlet manifold, the two lowest triplet states are of $n\pi^*$

($T_1$) and $\pi\pi^*$ ($T_2$) nature. Unfortunately, the information about these states is very scarce. In fact, the phosphorescence spectrum has not yet been detected even at 77 K, and absorption spectra did not reveal any band attributable to the singlet–triplet absorption. Furthermore, no triplet–triplet transient absorption, following pulsed laser excitation, has been observed up to now.

In this work, we consider the role of the torsional coordinate in the relaxation of Ab singlet excited states with the aim of clarifying the pathway of the $S_2$ decay and the nature of the observed intermediates. We also discuss the mechanism of the photoreactivity in the ground state and in the lowest triplet state that was so far mostly neglected both experimentally and theoretically. Aspects not considered in this work will be pursued elsewhere. The paper is organized as follows. We describe the computational techniques we employed in Sect. 2. We present our results, namely the potential-energy-curve diagram for the lowest singlet states, for the lowest triplet states and the vibrational frequencies for $S_1$, in Sect. 3. We discuss our results in the light of the observations and of previous calculations in Sect. 4.

## Computational details

The E–Z isomerization was studied using the CASSCF method, followed by multistate CAS second-order perturbation theory (MS-CASPT2) [26]. Comparative calculations were also performed with methods derived from DFT, using the B3LYP exchange–correlation functional [27].

For each value of the dihedral CNNC angle, the molecule's structure was optimized for the lowest singlet and triplet states at the DFT-B3LYP level. Using the B3LYP geometries, various singlet and triplet excited states were determined by reexploring these paths at the MS-CASPT2 and time-dependent (TD) DFT levels of theory. The most important structures along these curves were also optimized in the excited states at the CASSCF level of theory.

The CASSCF method [26] was used to generate molecular orbitals and reference functions for subsequent MS-CASPT2 calculations of the dynamic correlation energy [28]. The MS option of the CASPT2 method was employed: it allows CASPT2 calculations to be performed for a number of the selected roots from a state-average CASSCF calculation. An effective Hamiltonian, constructed using second-order perturbation theory, is diagonalized to obtain the final MS-CASPT2 energies [29]. The MOLCAS-5.2 quantum chemistry program [30] was used.

The choice of active space is a crucial step in a CASSCF calculation. In our previous study on the *trans*-stilbene molecule [31] we explored the performance of various active spaces up to the space formed by 14 valence $\pi$ molecular orbitals with 14 $\pi$ electrons. Ab is the analogue of stilbene, in which two nitrogen atoms have replaced the two central CH groups. In the Ab case, a calculation equivalent to the 14/14 calculation for stilbene would also include the two nitrogen bonding lone-pair orbitals, and this would add up to 18 electrons in 16 orbitals. It is presently not possible to handle such an active space. After a series of tests it turned out that a balanced active space is 14 electrons in 12 orbitals (14/12), corresponding to the 10/10 $\pi$ valence and the two doubly occupied nitrogen lone pairs.

In the $C_{2h}$ group of symmetry, the $\pi$ orbitals belong to the $A_u$ and $B_g$ irreducible representations. In the 14/12 calculation, the active space is composed of one, one, six and four active orbitals in the four irreducible representations $A_g$, $B_u$, $A_u$ and $B_g$, respectively. Results obtained with other active spaces, such as 14/14, in which two extra $\pi$ orbitals have been added to the 14/12 space, are also reported.

Generally, contracted basis sets of atomic natural orbital type were used with the contraction scheme 3s2p1d on C and N, and 2s1p on H [32].

The geometry of the ground state ($S_0$), the first singlet excited state ($S_1$) and the first triplet ($T_1$) excited state of *E*-Ab were optimized at the CASSCF level by computing analytical first derivatives [33]. The CASSCF harmonic frequencies for the $S_0$ and the $S_1$ states were computed using analytical second derivatives by the method of Bernhardsson et al. [34]. For comparison similar calculations were performed at the DFT-BLYP level, with a 6-31G* basis set, using the program Gaussian98.

## Results

### *Ground state*

The structure of the molecule and the numbering of the atoms are specified in Fig. 1. The energy differences between the *Z*-Ab and the *E*-Ab isomers are found to be 15.2 and 12.6 kcal $mol^{-1}$ by the B3LYP and the CASPT2 approaches, respectively. The experimental gap is about 12 kcal $mol^{-1}$ [35] and is quite close to the CASPT2 result. The Z and E isomers are separated by potential-energy barriers along both the torsional coordinate, along which the N = N bond is partially broken, and the in-plane inversion path, because the N hybridization changes from $sp^2$ to $sp$.

Experimentally [2, 36], it is found that thermal Z–E isomerization is associated with a barrier of 22–23 kcal $mol^{-1}$, i.e., the transition-state energy is about 35 kcal $mol^{-1}$ above the E isomer. Obviously, this value pertains to the energy of the lower of the two barriers, but experiments do not specify with which path it is associated.

The $S_0$ optimized potential-energy curve along the torsional path evaluated by B3LYP calculations is reported in Fig. 2. The transition-state energy along the inversion coordinate, calculated by the B3LYP approach, is 40.5 kcal $mol^{-1}$. Close to the transition-state geometry, one benzene ring becomes orthogonal to the molecular plane, as found by other authors [19, 37]. The torsional transition state corresponds to a biradicalic electronic structure; thus, nondynamical correlation energy is appreciable and the accurate estimate of its energy becomes more complicated. The calculation with the unrestricted B3LYP can give two different results corresponding to two different solutions. A transition-state energy of 49.4 kcal $mol^{-1}$ corresponding to $< S^2 > = 0$ is obtained, while an energy of 32.1 kcal $mol^{-1}$ corresponding to $< S^2 > = 1$ is found. The last solution indicates an equal-weight mixture of singlet and triplet diradicalic structures, which, in principle, should

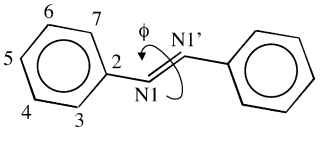


**Fig. 1.** The structure and the atom numbering of *trans*-azobenzene (Ab)

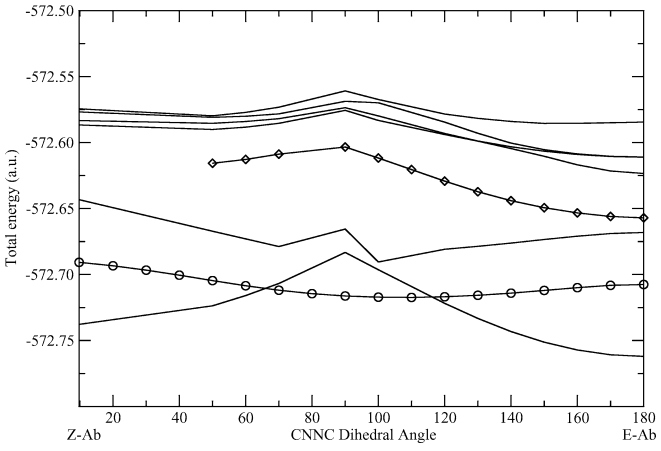


**Fig. 2.** Time-dependent density functional theory potential-energy curves along the NN twist. Singlet state energy curves (*full lines*); lowest triplet state ($T_1$) energy curve (*circles*); second lowest triplet state ($T_2$) energy curve (*diamonds*)

not be considered correct because of spin contamination. However, since the energy of the lowest triplet, at the same geometry, is 29 kcal $mol^{-1}$, i.e., very similar to the energy of the spin-contaminated state, the latter energy should be a good approximation to the energy of the $S_0$ torsional transition state. The CASPT2 calculations are certainly more significant in such a case and give a transition energy of 38.1 kcal $mol^{-1}$.

In conclusion, it appears from the present calculations that the transition states along the two isomerization paths have very similar energies, as suggested by Cimiraglia and Hoffmann [37], and that, contrary the suggestions of many authors, the N=N torsion is probably the path with the lower barrier. Furthermore, since the lowest triplet state, $T_1$, shows a still lower energy at a CNNC dihedral angle of 90° (29 kcal $mol^{-1}$ according to B3LYP), a contribution to the thermal process may come via a crossing to the triplet energy surface. This may render the torsional coordinate the more important for the thermal isomerization. In this respect, it is worth noting that the preexponential factor for thermal isomerization is about $10^{11}$ $s^{-1}$ [2, 36], definitely lower than the typical frequency factor $kT/h$ for adiabatic reactions.

We calculated the optimized geometries for the Z and E isomers. The typical bond distances, angles and rotational constants for the ground state ($S_0$) and the lowest singlet ($S_1$) and triplet ($T_1$) excited states of *E*-Ab, obtained at the CASSCF and B3LYP levels of theory, are reported in Table 1. For the $S_0$ ground state, B3LYP predicts bond distances in better agreement with experiment [20] than CASSCF. This is especially true for the central N=N double bond, which is predicted to be too short at the CASSCF level (1.239 versus 1.261 Å), with both the 14/12 and 14/14 active spaces. This result reflects the lack of the dynamical correlation in the CASSCF approach. A better description would require a CASPT2 or a MP2 optimization. The B3LYP geometries are, in general, reliable, and this is also the case for Ab as is seen from the data in Table 1.

Both CASSCF and B3LYP predict the CNNC and NNCC dihedral angles to be 0.0° for the E isomer. Interestingly, according to a MP2/6-31G* study [20], the NNCC angle corresponding to a minimum is different from zero and the potential-energy curve forms two minima at +19.5° and −19.5° separated by a tiny barrier of 0.4 kcal $mol^{-1}$. However, the presence of such a small barrier would not have a sharp physical consequence and the observed equilibrium geometry would still be planar.

The structural parameters calculated for the *Z* isomer are given in Table 2. With respect to the *E* isomer, the NC bonds are found to be longer by 0.01 Å by both the CASSCF and B3LYP approaches. The same result was found previously by Ishikawa et al. [21] and by Cattaneo and Persico [19]. The CNNC dihedral angle is predicted to be slightly different from zero, less than 10°, by both the CASSCF and B3LYP approaches. The NNCC dihedral angle is found to be about 50°, in agreement with the findings of most authors.

A comparison between the 14/12 and 14/14 CASSCF results shows little change in the N=N and N-C bond distances, indicating that even at the 14/12 level a good description of the structure is obtained.

**Table 1.** *Trans*-Azobenzene (*Ab*) bond lengths (Å) and angles (degrees)

| | B3LYP $S_0$ | CASSCF $S_0$[a] | CASSCF $S_0$[b] | Exp[c] | B3LYP $T_1$ | CASSCF $S_1$[a] |
|---|---|---|---|---|---|---|
| *r*(N1–N1′) | 1.261 | 1.239 | 1.239 | 1.260(8) | 1.261 | 1.253 |
| *r*(N1–C2) | 1.419 | 1.425 | 1.425 | 1.427(8) | 1.373 | 1.368 |
| *r*(C2–C3) | 1.401 | 1.395 | 1.392 | 1.401 | 1.411 | 1.410 |
| r(C3–C4) | 1.394 | 1.383 | 1.380 | 1.396 | 1.389 | 1.377 |
| *r*(C4–C5) | 1.396 | 1.396 | 1.401 | 1.397 | 1.400 | 1.400 |
| *r*(C5–C6) | 1.401 | 1.386 | 1.397 | 1.402 | 1.399 | 1.388 |
| *r*(C6–C7) | 1.390 | 1.394 | 1.390 | 1.393 | 1.390 | 1.387 |
| *r*(C2–C7) | 1.406 | 1.397 | 1.403 | 1.405 | 1.414 | 1.408 |
| ∠(N1′N1C2) | 114.80 | 114.97 | 115.01 | | 128.47 | 128.47 |
| ∠(N1C2C3) | 115.33 | 115.32 | 115.45 | 113.6(8) | 118.25 | 117.86 |
| ∠(N1C2C7) | 124.80 | 124.57 | 124.40 | 124.7(9) | 122.16 | 122.36 |
| *A* (GHz) | 2.732 | 2.759 | 2.756 | | 2.752 | 2.768 |
| *B* (GHz) | 0.292 | 0.293 | 0.293 | | 0.281 | 0.284 |
| *C* (GHz) | 0.264 | 0.265 | 0.264 | | 0.255 | 0.257 |

[a]14/12 active space
[b]14/14 active space
[c]Gas electron diffraction [20]

**Table 2.** *Cis*-Ab bond lengths (Å) and angles (degrees)

| | B3LYP $S_0$ | CASSCF $S_0$[a] | B3LYP $T_1$ |
|---|---|---|---|
| $r$(N1–N1′) | 1.250 | 1.237 | 1.295 |
| $r$(N1–C2) | 1.436 | 1.437 | 1.373 |
| $r$(C2–C3) | 1.401 | 1.380 | 1.416 |
| $r$(C3–C4) | 1.393 | 1.398 | 1.387 |
| $r$(C4–C5) | 1.397 | 1.393 | 1.401 |
| $r$(C5–C6) | 1.397 | 1.398 | 1.401 |
| $r$(C6–C7) | 1.393 | 1.381 | 1.388 |
| $r$(C2–C7) | 1.403 | 1.397 | 1.418 |
| ∠(N1′N1C2) | 124.08 | 122.52 | 122.49 |
| ∠(N1C2C3) | 116.39 | 117.48 | 117.31 |
| ∠(N1C2C7) | 123.05 | 121.73 | 123.52 |
| ∠(C2N1N1′C2′) | 9.78 | 2.95 | 107.48 |
| ∠(N1′N1C2C3) | 50.15 | 62.58 | 175.81 |
| $A$ (GHz) | 1.448 | 1.322 | 2.037 |
| $B$ (GHz) | 0.454 | 0.500 | 0.322 |
| $C$ (GHz) | 0.408 | 0.449 | 0.317 |

[a]14/12 active space

*Triplet state*

Experimental information about the energies and the properties of triplet states of Ab is very scarce. No solvent-induced absorption and emission $S_0$–$T_1$ transition has been observed, and no transient $T_n \leftarrow T_1$ absorption has been detected so far, even in low-temperature matrices. For comparison, in stibene $T_1 \rightarrow S_0$ phosphorescence and $T_n \leftarrow T_1$ transient absorption spectra could be observed [38]. The fact that $T_1$ has so far escaped observation underscores the very short lifetime of this state.

The only accurate determination of the energy of $T_1$ in both the Z and E isomers was carried out by Monti et al. [25], by an appropriate analysis of the rate constant for the energy transfer from a number of energy donors with different triplet energies. The adiabatic $T_1$–$S_0$ energy differences (corresponding approximately to the energy of the 0-0 band) for the E and Z isomers were found to be 35 and 29 kcal $mol^{-1}$, respectively. Taking into account that the adiabatic Z–E energy gap in $S_0$ is 12 kcal $mol^{-1}$, it follows that the absolute adiabatic energies of the E and the Z isomers in $T_1$ are 35 and 41 kcal $mol^{-1}$, respectively.

According to all calculations, the lowest triplet state in the planar geometries is of n$\pi^*$ nature. Once the molecule becomes nonplanar, following the N=N torsion, the n$\pi^*$ and $\pi\pi^*$ states mix and the weight of the $\pi\pi^*$ component increases twisting toward 90°.

The $T_1$ state energies, relative to the $S_0$ *E*-Ab energy, computed by the B3LYP approach at the most significant geometries, E, Z, inverted and twisted, are given in Table 3. After geometry-optimization the Z and E energies are 44.7 and 34.2 kcal $mol^{-1}$, respectively. These two structures prove to be transition states by frequency calculations. The optimized energies at the twisted and inverted geometries are 27.8 and 48.4 kcal $mol^{-1}$. It turns out that the latter geometry is not a transition state, but a second-order saddle point, while the former represents a minimum on the potential-energy surface. Thus, the inversion path for Z–E isomerization requires overcoming a barrier. In contrast, the torsion path leads monotonically to the minimum close to the twisted geometry, as found previously [18, 19], from where the decay to $S_0$ is very fast. Thus, the latter represents the more favorable path for triplet-state photoisomerization of Ab. As a check of the B3LYP results, we performed a CASPT2 calculation on the triplet energies and also these results, which are reported in Table 3, support the picture emerging from the B3LYP study.

**Table 3.** Energy differences (kcal/mol)

| | *E*-Ab | 90–100° | *Z*-Ab |
|---|---|---|---|
| DFT | | | |
| $S_0$ | 0.00 | 49.44 | 15.20 |
| $T_1$ | 34.19 | 28.01 | 44.73 |
| MSPT2 | | | |
| $S_0$ | 0.00 | 38.14 | 15.00 |
| $T_1$ | 42.26 | 28.82 | 50.74 |
| $S_1$vertical | 62.17 | 52.91 | |
| $S_2$vertical | 91.02 | 48.56 | |

The potential-energy curves of $S_0$ and $T_1$ along the torsional coordinates obtained by B3LYP are shown in Fig. 2. Interestingly, we find that the minimum of the $T_1$ potential-energy surface is not exactly above the $S_0$ barrier, but rather shifted somewhat toward the E isomer. This suggests that, by exciting both isomers in $T_1$, we should obtain predominantly the E form. Indeed, Bortolus and Monti [15] found by performing experiments of sensitized photoisomerization that the yield of the $E \rightarrow Z$ process is only 0.015, while the $Z \rightarrow E$ process occurs with a quantum yield of 1.

The crossings between the $T_1$ and $S_0$ potential-energy curves enable the thermal isomerization to proceed via a triplet state and enhance the rate of the $T_1 \rightarrow S_0$ intersystem crossing decay. Thus, the absence of spectroscopic observations of $T_1$ can be related to the very short lifetime of this state caused by the $T_1/S_0$ crossings.

The second triplet state is of $\pi\pi^*$ character at the twisted geometry and shows a high barrier at about 90° along the NN twisting [18, 19]. It was inferred [18] that this barrier is due to the n$\pi^*$ component, which becomes dominant as rotation proceeds. We calculated the potential-energy curves of a number of triplet states at the $T_1$ geometries by the TD-DFT procedure. The results are reported in Fig. 2. It appears that the second triplet state is much higher than $T_1$ and vestiges of potential-energy crossing between the $\pi\pi^*$ and n$\pi^*$ diabatic components cannot be recognized. Furthermore, the substantially higher energy of $T_2$ rules out the possibility that this state plays a role in the sensitized photoisomerization experiments performed so far.

*Excited singlet states*

As discussed in the Introduction, the UV–vis absorption spectrum of *E*-Ab in hexane solution shows a weak band at 432 nm ($\epsilon_{max} = 400$) and an intense band with a maximum at 318 nm ($\epsilon_{max} = 22{,}300$). The former is structureless even in low-temperature mixed crystals and is attributed to the lowest singlet state, $S_1(B_g)$ of $n\pi^*$ nature. The latter is attributed to $S_2(B_u)$ of $\pi\pi^*$ nature and shows a vibronic structure exhibiting identifiable vibrational progressions in the dibenzyl single-crystal spectrum.

The lifetime of the $S_2$ state was found to be very short, 0.1 ps, while the lifetime of $S_1$ was found to vary from 2.5 to 0.5 ps depending on the excitation wavelength used. Unfortunately, no lifetime measures have been performed in a situation where one of the two isomerizable coordinates is kept fixed, such as in rigid matrices or in sterically hindered Ab derivatives.

According to previous studies of potential-energy diagrams [18, 19], the inversion coordinate alone cannot explain the short lifetime of $S_2$ or the wavelength-dependence of the Ab photophysical properties. For this reason we reexamined the potential-energy curves for the NN twisting path of isomerization in a number of low-lying singlet states.

The energies of the lowest excited singlet states were calculated at the MS-CASPT2 level, in the planar E geometry optimized for the $S_0$ state. These energies are reported in Table 3. The $S_1(n\pi^*)$ and the $S_2(\pi\pi^*)$ states are found at 2.7 and 3.9 eV, respectively, in good agreement with the energies of 2.9 and 3.9 eV corresponding to the maxima (432 and 318 nm) observed in the UV–vis absorption spectra. Only 5 kcal $mol^{-1}$ above $S_2$ we find a state of type $A_g$ in which the main electronic configuration is the $n^2\pi^{*2}$ double excitation, in agreement with the calculation of Ref. [19].

The optimized geometry of the $S_1$ state, calculated by the 14/12 CASSCF approach with the 14/12 active space, assuming $C_{2h}$ symmetry as in the ground state, is reported in Table 1. With respect to the ground-state-geometry parameters, the NN bond is slightly longer in $S_1$, by 0.014 Å, while the NC bonds shorten significantly, by 0.057 Å. The NNC angle increases from 115° in the ground state to about 128°. The variations indicate that in $S_1$ the NN bond order is similar to that in the ground state and that the decrease of the n orbital electronic population favors the *sp* hybridization and makes it easier for the molecule to isomerize along the in-plane inversion path.

The potential-energy curves along the NN torsional coordinate from E toward Z geometry, calculated with the TD-DFT and the MS-CASPT2 approaches, are reported in Figs. 2 and 3, respectively. The energy curves of excited singlet states are calculated at 10° intervals for the optimized geometries of the ground state.

The TD-DFT energy curves displayed in Fig. 2 include only singly excited states, since this method does not take into account properly doubly excited states. No singly excited state shows a clear minimum at 90° twisted geometry. Furthermore, these curves fail to reveal any feature that can explain the fast decay of $S_2$ and the ability of this state to decay bypassing $S_1$.

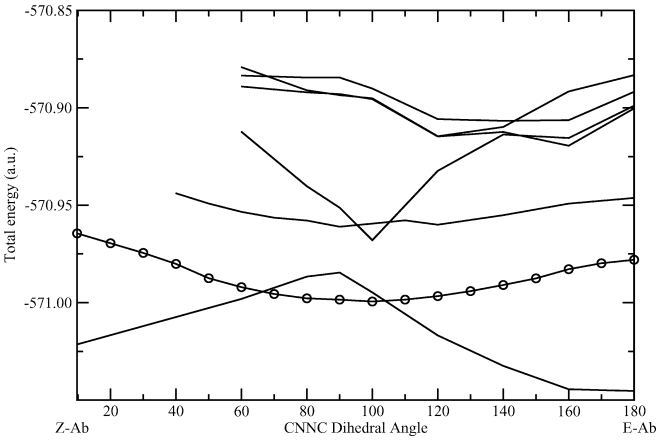


**Fig. 3.** The complete-active space second-order perturbation theory potential-energy curves along the NN twist curves. Singlet energy curves (*full lines*); lowest triplet state energy curve (*circles*)

The potential-energy curve of $S_1$ shows peculiar behavior in the twisted region that may be an artifact of the TD-DFT method in the region of 90°, where $S_1$ has a small energy gap with respect to $S_0$. Thus, the TD-DFT energy curves of excited singlet states are not very useful to analyze the photochemistry and the photophysics of Ab.

The vertical potential-energy curves calculated by the MS-CASPT2 approach, at the optimized ground-state geometries, are reported in Fig. 3. These curves pertain to the lowest six singlet states, including doubly excited states that are usually important for the photochemical reactions although they are not observed by the usual one-photon absorption spectroscopy. The $S_1$ energy curve along the NN torsion is essentially flat and geometry-optimization starting from a twisted geometry brings the molecule back toward the E geometry. All the other excited-state energy curves, with the exception of $S_3$, do not exhibit minima at the twisted geometry, but rather at about 140°, above the E isomer geometry. Thus, they should not induce appreciable $E \rightarrow Z$ photoisomerization, and are compatible with a very high $Z \rightarrow E$ photoisomerization. This holds in particular for the $S_2(\pi\pi^*)$ state. The $S_3$ state, of $A_g$ symmetry and based predominantly on the $n^2\pi^{*2}$ doubly excited configuration in the planar geometry, shows a potential-energy curve with a deep minimum at about 100°, close to the twisted geometry, as found by Cattaneo and Persico [19]. According to our calculations, the energy curve of this state crosses not only the $S_2$ energy curve, but also the $S_1$ energy curve, becoming at the 100° twisted geometry the lowest singlet excited state with an energy lower by about 5 kcal $mol^{-1}$ than the $S_1$ state. We checked that the doubly excited state remains below the $S_1(n\pi^*)$ state after geometry-optimization. This $S_3$ state obviously plays a fundamental role in the decay of

**Table 4.** $A_g$ vibrational frequencies ($cm^{-1}$) for the $1^1A_g$ and $1^1B_g$ states of *trans*-Ab (symmetry group $C_{2h}$)

| Mode | $S_0$ | | | | $S_1$ |
|---|---|---|---|---|---|
| | BLYP | CASSCF[a] | Exp[b] | Assignment[c] | CASSCF[a] (Exp[d]) |
| $\nu$23 | 215.8 | 216 | 218 | NNC bend | 189 |
| $\nu$22 | 297.9 | 293 | 362 | NCC bend | 285 |
| $\nu$21 | 609.7 | 603 | 611 | CCC bend | 600 |
| $\nu$20 | 664.5 | 652 | 667 | CCC bend | 639 (635) |
| $\nu$19 | 907.2 | 904 | – | CCC bend + NNC bend | 823 (845) |
| $\nu$18 | 987.5 | 981 | 1,000 | CC stretch (1) + CCC bend | 963 |
| $\nu$17 | 1,015.1 | 1,010 | 1,021 | CCH wag (18a) + CCC bend | 972 (980) |
| $\nu$16 | 1,072.1 | 1,061 | 1,068 | CCH wag (18b) | 1,010 |
| $\nu$15 | 1,121.8 | 1,094 | 1,143 | NC stretch + CCH wag (13/9a) | 1,073 |
| $\nu$14 | 1,162.3 | 1,140 | 1,155 | CCH wag (9b) | 1,112 (1130) |
| $\nu$13 | 1,178.6 | 1,174 | 1,185 | CCH wag (9a) + NC stretch | 1,158 |
| $\nu$12 | 1,308.9 | 1,224 | – | CCH wag + NC stretch | 1,193 |
| $\nu$11 | 1,341.1 | 1,311 | 1,312 | CC stretch (14) | 1,311 |
| $\nu$10 | 1,400.1 | 1,443 | 1,440 | NN stretch | 1,438 (1,428) |
| $\nu$9 | 1,466.6 | 1,482 | 1,470 | CC stretch (19b) + NN stretch | 1,462 |
| $\nu$8 | 1,483.7 | 1,554 | 1,491 | CC stretch (19a) + NN stretch | 1,551 (1,550) |
| $\nu$7 | 1,576.3 | 1,578 | – | CC stretch (8a/b) | 1,572 |
| $\nu$6 | 1,591.9 | 1,601 | 1,591 | CC stretch (8a/b) | 1,609 |

[a] Frequencies multiplied by scaling factor 0.91
[b] From Ref. [40]
[c] In parentheses benzene modes parentage
[d] From Ref. [23]

**Table 5.** $B_g$ vibrational frequencies ($cm^{-1}$) for the $1^1A_g$ and $1^1B_g$ states of *trans*-Ab (symmetry group $C_{2h}$)

| Mode | $S_0$ | | | | S1 |
|---|---|---|---|---|---|
| | BLYP | CASSCF[a] | Exp[b] | Assignment[c] | CASSCF |
| $\nu$33 | 107.2 | 73 | – | NC tors | 148 |
| $\nu$32 | 246.2 | 238 | 250 | NC flap | 347 |
| $\nu$31 | 408.5 | 408 | 406 | Ring op def | 411 |
| $\nu$30 | 475.6 | 468 | – | Ring op def | 502 |
| $\nu$29 | 676.1 | 671 | 689 | Ring op def | 668 |
| $\nu$28 | 756.6 | 747 | 773 | CH op bend (11) | 737 |
| $\nu$27 | 835.0 | 828 | 834 | CH op bend (10a) | 812 |
| $\nu$26 | 912.1 | 906 | 914 | CH op bend (17b) | 875 |
| $\nu$25 | 943.8 | 977 | 935 | CH op bend (5) | 975 |
| $\nu$24 | 966.6 | 998 | 967 | CH op bend (17a) | 987 |

[a] Frequencies multiplied by scaling factor 0.91
[b] From Ref. [40]
[c] In parentheses benzene modes parentage

the $S_2$ state and is very similar in its electronic structure and in its effect to the $HOMO^2 \rightarrow LUMO^2$ $A_g$ state of stilbene with a potential-energy minimum at 90° [39]. The molecule after excitation in $S_2$ can reach $S_3$ without activation energy via a conical intersection and from this state can reach the ground state or, via conical intersection, the $S_1$ state.

We characterized the minima of the $S_1$ state by calculating their vibrational frequencies with the purpose of assigning the transient resonance Raman spectrum measured by Fujino and Tahara [23]. To calculate the harmonic force field of $S_1$ we used the CASSCF approach, with the 14/12 active space, and scaled the vibrational frequencies by the factor 0.91 to take into account the effect of dynamic correlation neglected by the CASSCF on the force field. To determine this factor we compared the ground-state frequencies obtained by the same CASSCF approach and by the accurate DFT-BLYP method. The $S_0$ and $S_1$ calculated frequencies are reported in Tables 4, 5, 6 and 7, together with the experimental frequencies [23, 40].

The BLYP ground-state frequencies appear to describe quite accurately the observed frequencies as did previous calculations with the PW91/6-31 + G* and BP86/6-31G* DFT versions [41] and the MP2 approach [42]. Most of the $S_0$ experimental frequencies can be assigned on the basis of calculations, taking into account not only the frequencies, but also IR intensities and Raman depolarization ratios. The scaled CASSCF frequencies represent satisfactorily the observed ground-state frequencies [41]. Thus, the $S_1$ frequencies calculated in the same way, reported in the same tables, should allow us to represent correctly the vibrational frequencies observed in the transient Raman spectrum [23]. The good correspondence between observed and calculated $S_1$ frequencies provides strong support to the hypothesis that the transient state responsible for the time-resolved Raman spectra is the $S_1$ state.

## Discussion

The main results of the present CASPT2 calculations are summarized in Fig. 3, which shows the potential-energy curves along the NN torsional coordinate of the lowest singlet states. The most important finding is the potential-energy curve of the $S_3(n^2\pi^{*2})$ state, which shows a deep minimum at 100°, at the twisted geometry, con-

**Table 6.** $A_u$ vibrational frequencies ($cm^{-1}$) for the $1^1A_g$ and $1^1B_g$ states of *trans*-Ab (symmetry group $C_{2h}$)

| Mode | $S_0$ | | | | S1 |
|---|---|---|---|---|---|
| | BLYP | CASSCF[a] | Exp[b] | Assignment[c] | CASSCF |
| $\nu$44 | 25.5 | 18 | – | NC tors | $i$10 |
| $\nu$43 | 60.2 | 61 | – | NC flap + ring op def | 53 |
| $\nu$42 | 296.4 | 300 | 315 | NN tors + ring op def (16b) | 221 |
| $\nu$41 | 405.1 | 406 | 409 | Ring op def (16a) | 408 |
| $\nu$40 | 540.7 | 534 | 544 | NN tors + ring op def | 466 |
| $\nu$39 | 682.8 | 680 | 690 | Ring op def + CH op bend | 665 |
| $\nu$38 | 774.3 | 762 | 774 | CH op bend (11) | 733 |
| $\nu$37 | 834.3 | 827 | 834 | CH op bend (10a) | 810 |
| $\nu$36 | 916.5 | 909 | 926 | CH op bend (17b) | 875 |
| $\nu$35 | 943.8 | 977 | 967 | CH op bend (5) | 974 |
| $\nu$34 | 996.8 | 998 | 983 | CH op bend (17a) | 987 |

[a] Frequencies multiplied by scaling factor 0.91
[b] From Ref. [40]
[c] In parentheses benzene modes parentage

**Table 7.** $B_u$ vibrational frequencies ($cm^{-1}$) for the $1^1A_g$ and $1^1B_g$ states of *trans*-Ab (symmetry group $C_{2h}$)

| Mode | $S_0$ | | | | S1 |
|---|---|---|---|---|---|
| | BLYP | CASSCF[a] | Exp[b] | Assignment[b] | CASSCF |
| $\nu$66 | 82.4 | 82 | 86 | NCC bend + NNC bend | 54 |
| $\nu$65 | 515.5 | 507 | 523 | NNC bend + NCC bend | 445 |
| $\nu$64 | 531.5 | 527 | 544 | CCN bend + CCC bend | 515 |
| $\nu$63 | 615.3 | 609 | 617 | CCC bend | 610 |
| $\nu$62 | 811.3 | 801 | – | CCC bend | 810 |
| $\nu$61 | 987.3 | 981 | 1,000 | CC stretch + CCH wag (12) | 966 |
| $\nu$60 | 1,015.1 | 1,010 | 1,021 | CCH wag 18a | 1,007 |
| $\nu$59 | 1,076.1 | 1,064 | 1,070 | CCH wag 18b | 1,069 |
| $\nu$58 | 1,148.6 | 1,111 | 1,155 | CCH wag 9b | 1,118 |
| $\nu$57 | 1,162.3 | 1,138 | 1,181 | CCH wag 9a | 1,163 |
| $\nu$56 | 1,213.0 | 1,220 | 1,218 | CN stretch + CCH wag (9a) | 1,200 |
| $\nu$55 | 1,304.8 | 1,229 | 1,295 | CCH wag (3) | 1,295 |
| $\nu$54 | 1,338.7 | 1,307 | 1,307 | CC stretch (14) | 1,405[d] |
| $\nu$53 | 1,453.5 | 1,443 | 1,454 | CC stretch (19b) | 1,456 |
| $\nu$52 | 1,482.8 | 1,489 | 1,484 | CC stretch (19a) | 1,527 |
| $\nu$51 | 1,572.8 | 1,578 | 1,586 | CC stretch (8a/b) | 1,559 |
| $\nu$50 | 1,590.3 | 1,590 | 1,591 | CC stretch (8a/b) | 2,840[d] |

[a] Frequencies multiplied by scaling factor 0.91
[b] From Ref. [40]
[c] In parentheses benzene modes parentage
[d] Anomalously high values owing to a numerical artifact

firming the CIPSI result of Ref. [19]. According to our CASPT2 calculations, the $S_3$ state lies about 5 kcal $mol^{-1}$ above $S_2$ at the E geometry. Its energy curve crosses the $S_2$ potential-energy curve close to the E geometry, in the Franck–Condon region of the $S_2 \leftarrow S_0$ transition, and no activation energy is required to reach the crossing from the excited E $S_2$. A key feature of the $S_3$ energy curve is that its minimum is found below the $S_1(n\pi^*)$ potential-energy curve and at the twisted geometry of 100°, i.e., closer to the E geometry. Thus the $S_3$ energy curve also crosses the $S_1$ energy curve. The $S_3$ potential-energy curve along the NN torsion provides a fast decay path for the deactivation of the $S_2$ state.

The consequences on the photophysical/photochemical properties of Ab excited in the $S_2$ state are the following: (1) the $S_2 \rightarrow S_3$ radiationless transition occurs via conical intersection and, thus, is extremely fast, certainly faster than the vertical $S_2 \rightarrow S_1$ decay taking place at the E geometry; (2) once on the $S_3$ energy surface, the molecule reaches the $S_1/S_3$ conical intersection and jumps on the $S_1$ energy surface or reaches the minimum of the $S_3$ energy surface and then decays to the ground state. In the latter case, since the minimum of the $S_3$ energy surface is not at 90°, but is displaced toward the E geometry, $S_3 \rightarrow S_0$ decay does not contribute to the $E \rightarrow Z$ isomerization. In the former case, after reaching the $S_1$ state, the molecule will isomerize with the quantum yield and according to the proper mechanism of this state. Thus, because of the fast $S_2 \rightarrow S_3$ radiationless transition and of the branching of the following decay, excitation in $S_2$ will give a lower photoisomerization quantum yield than excitation in $S_1$. In this way, the wavelength-dependence of the photoisomerization quantum yield of Ab is explained. The pathways for the decay from the $S_2$ state are shown in Fig. 4.

When the motion along the torsional coordinate is blocked, the molecule excited in $S_2$ cannot reach the $S_3$ state, but can decay only to $S_1$ at a planar geometry. Consequently, the photoisomerization quantum yield for excitation of $S_2$ and $S_1$ will be the same, as found for the azobenzenophanes [2]. Thus the non-Kasha behavior disappears in these Ab derivatives. At the same time, the $S_2$ lifetime of these compounds is expected to become longer than 0.11 ps, the lifetime of free Ab. Experimental support for this inference is provided by the linewidth of the $S_2 \leftarrow S_0$ absorption spectra in bibenzyl crystals at 20 K [14], where the matrix effects keep Ab planar. The linewidth of vibronic bands, which was

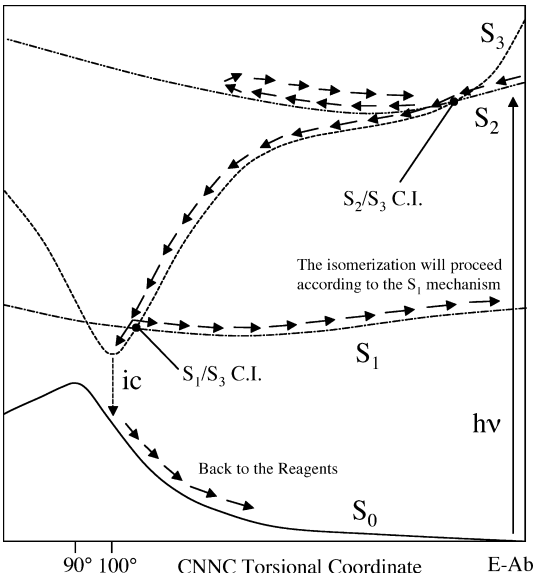


**Fig. 4.** Mechanism of $S_2$ decay in free Ab. Energy curves are schematized for the sake of clarity

found to be 50 $cm^{-1}$, corresponds to an $S_2$ lifetime of 0.6 ps that is 5–6 times longer than the $S_2$ lifetime measured in room-temperature fluid solutions.

We did not investigate the mechanism of the fast $S_1$ decay considering also the inversion coordinate. The search for critical geometries in a coordinate space not limited to the NN twisting is necessary for this. From the CASPT2 energy curve shown in Fig. 3 it is not obvious that E $\rightarrow$ Z isomerization may occur in $S_1$. Previous theoretical work [18, 19] indicates that $S_1$ photoisomerization can follow the inversion path. The transient Raman spectrum observed after excitation of the $S_2$ state [23] has been shown to be compatible with the $S_1$ vibrational frequencies. This assignment supports the notion that after excitation to $S_2$ a significant amount of $S_1$ is formed.

The present calculations show that the potential-energy curve of the triplet $T_1$ has a minimum of 27.8 kcal $mol^{-1}$ in the twisted region and thus indicate that photoisomerization of this state can occur along the NN twisting path. On the other hand, the energy of the transition state along the inversion coordinate is found at much higher energy, 48.4 kcal $mol^{-1}$. It follows that Ab Z $\rightarrow$ E isomerization in the $T_1$ state can occur only along the NN twisting path. Experiments of sensitized photoisomerization in rigid Ab derivatives, in which the NN twisting is blocked, would be useful to test this conclusion.

Further work considering both isomerization coordinates is under way and will be presented elsewhere.

*Acknowledgement* The financial support from MIUR (project "Modellistica delle proprietà spettroscopiche di sistemi molecolari complessi" funds ex 60% and project "Dinamiche molecolari in sistemi di interesse chimico" funds ex 40%), from the University of Bologna (Funds for Selected Research Topics) is gratefully acknowledged.

## References

1. (a) Zimmermann G, Chow LY, Park UI (1958) J Am Chem Soc 80:3528; (b) Gegiou D, Muszkat KA, Fischer E (1968) J Am Chem Soc 90:12
2. Rau H, Luddeke E (1982) J Am Chem Soc 104:1616
3. Rau H (1990) In Dürr H, Bounas-Laurent H (eds) Photochroism, molecules and systems, vol 1. Elsevier, Amsterdam, pp 165–192
4. Ikeda T, Tsutsumi O (1995) Science 268:1873
5. Willner I, Rubin S, Riklin A (1995) J Am Chem Soc 113:3321
6. Liu ZF, Hashimoto K, Fujishima K (1990) Nature 347:658
7. Hugel T, Holland NB, Cattani A, Moroder L, Seitz M, Gaub HE (2002) Science 296:1103
8. Griffiths J (1972) Chem Soc Rev 1:41
9. Rau H (1973) Angew Chem Int Ed Engl 12: 224
10. Lednev I, Ye TQ, Matousek P, Townie M, Foggi P, Neuwahl F, Umapathy S, Hester R, Moore J (1998) Chem Phys Lett 290:68
11. Nagële T, Hoche R, Zinth W, Wachtveitl J (1997) J Chem Phys 106:519
12. Lednev I, Ye TQ, Hester R, Moore J (1996) J Phys Chem 100:13338
13. Hochstrasser RM, Lower SK (1962) J Chem Phys 36:3505
14. Dick RH, McClure DS (1962) J Chem Phys 36:2326
15. Bortolus P, Monti S (1979) J Phys Chem 83:648
16. Siampiringue N, Guyot G, Bortolus P, Monti S (1987) J Photochem 37:185
17. Fujino T, Arzhantsev SY, Tahara T (2001) J Phys Chem A 105:8123
18. Monti S, Orlandi G, Palmieri P (1982) Chem Phys 71:87
19. Cattaneo P, Persico M(1999) Phys Chem Chem Phys 1:4739
20. Tsuji T, Takashima H, Takeuchi H, Egawa T, Konaka S (2001) J Phys Chem A 105:9347
21. Ishikawa T, Noro T, Shoda T (2001) J Chem Phys 115:7503
22. Hättig C, Hald K (2002) Chem Phys Phys Chem 4:2111
23. Fujino T, Tahara T (2000) J Phys Chem A 104:4203
24. Morgante OG, Struve WS (1979) Chem Phys Lett 68:267
25. Monti S, Gardini E, Bortolus P, Amouyal E (1981) Chem Phys Lett 77:115
26. Roos BO (1987) In: Lawley KP (ed) Advances in Chemical physics; ab initio methods in quantum chemistry–II. Wiley, Chichester, p 399
27. (a) Becke AD (1993) J Chem Phys 98:5648; (b) Lee C, Yang W Parr RG (1988) Phys Rev B37:785
28. (a) Andersson K, Malmqvist P-Å, Roos BO, Sadlej AJ, Wolinski K (1990) J Phys Chem 94:5483; (b) Andersson K, Malmqvist P-Å, Roos BO (1992) J Chem Phys 96:1218; (c) Roos BO, Andersson K, Fülscher, MP, Malmqvist P-Å, Serrano-Andrés L, Pierloot K, Merchán M (1996) In Prigogine I, Rice SA (eds) Advances in chemical physics: new methods in computational quantum mechanics, vol XCIII. Wiley, New York, p 219
29. Finley J, Malmqvis P-Å, Roos BO, Serrano-Andrés L (1998) Chem Phys Lett 288:299
30. Andersson K, Barysz M, Bernhardsson A, Blomberg MRA, Carissan Y, Cooper DL, Cossi M, Fleig T, Fülscher MP; Gagliardi L, de Graaf C, Hess BA, Karlström G, Lindh R, Malmqvist P-Å, Neogrády P, Olsen J, Roos BO, Schimmelpfennig B, Schütz M, Seijo L, Serrano-Andrés L, Siegbahn PEM, Stålring J, Thorsteinsson T, Veryazov V, Wierzbowska M, Widmark P-O (2001) MOLCAS version 5.2. Department of Theoretical Chemisty, University of Lund, Lund, Sweden
31. Gagliardi L, Orlandi G, Molina V, Malmqvist P, Roos BO (2002) J Phys Chem A 106:7355
32. Pierloot K, Dumez B, Widmark P-O, Roos BO (1995) Theor Chim Acta 90:87
33. Lindh R (1993) Theor Chim Acta 85:423
34. Bernhardsson A, Lindh R, Olsen J, Fülscher M (1999) Mol Phys 96:617

35. Adamson AW, Vogler A, Kunkely H, Wachter R (1978) J Am Chem Soc 100:1300
36. Brown EV, Grunneman GR (1975) J Am Chem Soc 97:621
37. Cimiraglia R, Hoffmann HJ (1994) Chem Phys Lett 217:430
38. Goerner H, Schulte-Frohlinde D (1981) J Phys Chem 85:1835
39. Orlandi G, Siebrand W (1975) Chem Phys Lett 30:352
40. Gruger A, LeCalve N, Dizabo P (1972) J Chim Phys 69:291
41. Kurita N, Tanaka S, Itoh S (2000) J Phys Chem A 104:8114
42. Armstrong DR, Clarkson J, Smith WE (1995) J Phys Chem 99:17825